

# Contact-timing and Trajectory Optimization for 3D Jumping on Quadruped Robots

Chuong Nguyen and Quan Nguyen

**Abstract**—Performing highly agile acrobatic motions with a long flight phase requires perfect timing, high accuracy, and coordination of the whole body motion. To address these challenges, this paper presents a unified timing and trajectory optimization framework for legged robots performing aggressive 3D jumping. In our approach, we firstly utilize an effective optimization framework using simplified rigid body dynamics to solve for contact timings and a reference trajectory of the robot body. The solution of this module is then used to formulate a whole-body trajectory optimization based on the full nonlinear dynamics of the robot. This combination allows us to effectively optimize for contact timings while guaranteeing the accuracy of the jumping trajectory that can be realized in the hardware. We validate the efficiency of the proposed framework on the A1 robot model for various 3D jumping tasks such as double-backflips and double barrel roll off the high altitude of  $2m$  and  $0.8m$  respectively. Experimental validation was also successfully conducted for different 3D jumping motions such as barrel roll from a box or diagonal jumps.

## I. INTRODUCTION

The last two decades have seen the rapid research and development of legged robots to traversing rough terrain [1],[2],[3],[4],[5]. Among them, the research into jumping behaviors on legged robot has greatly drawn research attentions because of its remarkable advantages to navigate high obstacles [6],[7],[8],[9]. With recent advancement of hardware and well-established control strategies, quadruped robots has shown its impressive capabilities to perform various dynamic locomotion [10],[11],[12]. Regarding to jumping behaviors, the Cheetah 2 recently demonstrates jumping autonomously over obstacles while bounding at high-speed [7], and the Cheetah 3 is able to repeatably jump onto and jump down from a desk up to  $30''$  in height [13].

The idea of simplifying its complex dynamics model as a single rigid body (SRB) dynamics model has been widely used to implement control algorithms for dynamics locomotion. In this model, legs and trunk are lumped into a unified single rigid body, in which its orientation and CoM position are directly influenced by the ground reaction forces (GRF). Utilizing this model via Model Predictive Control (MPC), [14] has obtained robust quadruped locomotion with a large number of gaits such as bound, pronk, pace and gallop. Recent development in [12] integrated the MPC controller with whole-body impulse control to achieve more robustness and versatility in these gaits and high speed running with the Mini-Cheetah robot. Specifically related

This work is supported by USC Viterbi School of Engineering startup funds.

The authors are with the Department of Aerospace and Mechanical Engineering, University of Southern California, USA: vanchuong.nguyen@usc.edu, quann@usc.edu,

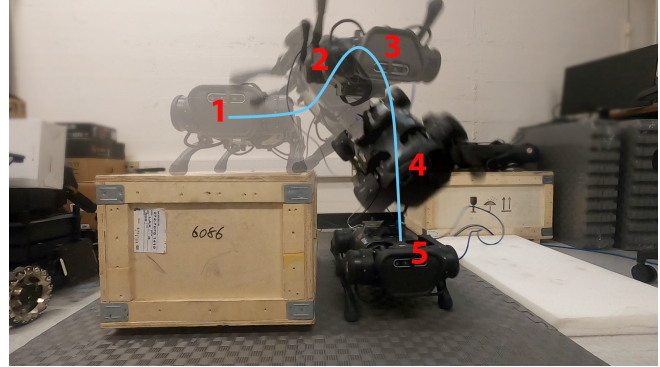


Fig. 1: A barrel roll on the A1 robot with our proposed framework.

to jumping behaviors, [15] presents an MPC framework for 3D jumping by linearizing the rigid body dynamics along with rotation matrix. However, to guarantee real-time computation of the MPC control in this work, the prediction horizon is limited, which affects jumping motions with a long flight phase. Therefore, in this paper, we are interested in the trajectory optimization (TO) to solve for complex acrobatic motions with a long flight phase. Our proposed approach includes trajectory optimization for the whole body dynamics (WBD) model, and develop a method to compute contact timings for various 3D jumping motions. The trajectory optimization approach is also used in [16] to optimize for gait and trajectories through phase-based parametrization. However, this also uses a linearized rigid body dynamics using Euler angle representation for their framework. Our method instead uses full nonlinear dynamics in the trajectory optimization framework to achieve highly accurate 3D jumping. We also include a contact-timing optimization approach using rigid body dynamics but based on a rotation matrix to represent 3D orientation to avoid singularity. The contact timing approach also allows us to find a jumping trajectory with a minimal effort or energy, guaranteeing successful hardware transfer.

When performing highly dynamic jumping, it is critical to utilize the full nonlinear dynamics of the robot to maximize the jumping performance as well as guarantee the accuracy of the jumping trajectory while realizing in the real robot hardware. Our previous work [13] simplifies the whole-body dynamics into 2D with 7 degree of freedom, then implements successfully the jumping on the MIT Cheetah 3 robot. Extending this to 3D jumping behaviors is challenging due to the complexity of the model, a highly nonlinear dynamic constrains, and a large number of other constraints related to joints' kinematics, torque, configuration and obstacles clearance. A recent work [9] proposes a framework

that implements trajectory optimization using a centroidal dynamics with kinematic constraints, then uses a whole-body controller that tracks the reference motions, instead of directly implementing the trajectory optimization of the whole-body dynamics. In both [9] and [13], the contact timings are manually tuned with respect to different jumping motions. Difference than [9] and [13], our work address the whole-body trajectory optimization (whole-body TO) for 3D jumping with optimized contact timings.

The contribution of the work is summarized as follows:

- Firstly, we present the whole-body TO to perform various 3D jumping tasks. To the best of our knowledge, our work is the first demonstration which obtained from that approach for 3D jumping behaviors on quadruped robots on the real hardware.
- Secondly, we propose a TO approach based on SRB to solve for optimal contact timings and reference trajectory of robot body in a fast manner, which will be used for the whole-body TO. In addition, since we directly use rotation matrix, we provide a solution to plan a wide range of 3D motions for SRB-based robots such as quadcopters, in which singularity and unwinding issues avoidance are important [17].
- The efficiency of the proposed framework is validated on the A1 robot model for various aggressive 3D jumping tasks, e.g., double-backflips and double barrel roll off boxes of height 2m and 0.8m correspondingly.
- We also validate the advantage of the framework via successful experiments for different 3D jumping motions such as diagonal jumps or barrel roll from a box.

The rest of our paper is organized as follows. Section II describes the robot we implement the proposed framework. The TO approaches are presented in Section III, and jumping and landing controller are briefly described in Section IV. Results from selected hardware experiments are shown in Section V. Finally, Section VI provides concluding remarks.

## II. HARDWARE PLATFORM

We validate our proposed framework on the Unitree’s A1 robot (see Fig. 2). It has high torque density electric motors with single-stage 9:1 planetary gear reduction, and uses these actuators for all the hip, thigh, and knee joints to enable full 3D control of GRF. A pressure-based contact sensor is equipped on each foot. The A1 legs feature a large range of motion: the hip joints have a range of motion of  $\pm 46^\circ$ , the thigh joints have a range of motion from  $-60^\circ$  to  $240^\circ$  and the knee joints have a range from  $-154.5^\circ$  to  $-52.5^\circ$ . The hip and knee designs allow the robot to operate identically forward, backward and flipped upside-down. The lower link is driven by a bar linkage which passes through the upper link. The robot parameters and its actuation capabilities are summarized in Table I. In the next sections, we present the development of the framework.

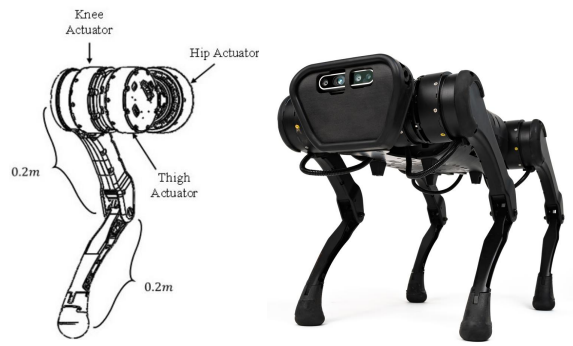


Fig. 2: **A1 robot.** Each leg consists of three actuators.

TABLE I: A1 Robot Parameters

| Parameter        | Symbol                   | Value               | Units             |
|------------------|--------------------------|---------------------|-------------------|
| Gear Ratio       | $gr$                     | 9                   |                   |
| Max Torque       | $\tau_{max}$             | 33.5                | Nm                |
| Max Joint Speed  | $\dot{q}_{max}$          | 21                  | rad/s             |
| Total leg mass   | $m_l$                    | 4.71                | kg                |
| Total robot mass | $m$                      | 12                  | kg                |
| Trunk dimension  | $l, w, h$                | 0.361, 0.194, 0.114 | m                 |
| Trunk Inertia    | $I_{xx}, I_{yy}, I_{zz}$ | 0.017, 0.056, 0.065 | kg.m <sup>2</sup> |
| Hip Link Lengths | $l_1$                    | 0.083               | m                 |
| Leg Link Lengths | $l_2, l_3$               | 0.2                 | m                 |

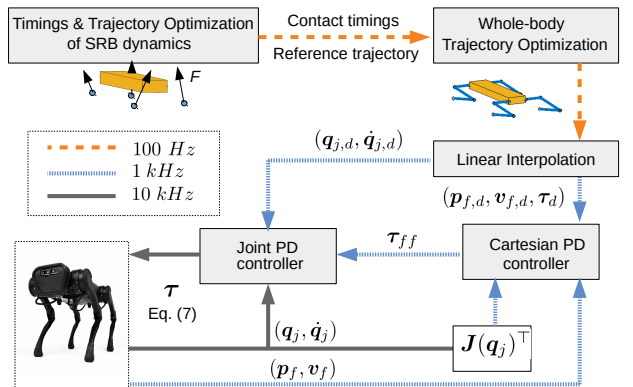


Fig. 3: **Block Diagram for the propose framework.** The timings and TO of SRB dynamics produces the contact timings and reference trajectory at 100 Hz for the TO of whole-body dynamics. Linear interpolation is then used to get the reference profile at 1 kHz for the Cartesian controller. The joint PD controller executes at 10 kHz.

## III. TRAJECTORY OPTIMIZATION WITH CONTACT TIMINGS OPTIMIZATION

In this Section, we present a new approach to extend our previous work [13] in 2D jumping to 3D jumping. In addition, we also introduce contact-timing optimization into our framework. Due to the high complexity of the problem, the feasible domain is limited. Thus, it is necessary to have a reference trajectory that we use to guide the whole-body TO converge to a feasible solution. Moreover, since the feasibility of the domain crucially depends on the selection of contact timings, we need to select appropriate contact timings. Because the manual selection of the timings to have

a feasible solution in the whole-body TO is a trial and error, and time-consuming task, it is very important to implement an approach to automatically compute optimal timings. In addition, timings in highly dynamic acrobatic motion with long flight phase play a crucial role in minimizing the effort or energy, guaranteeing the feasibility of the motion within the limit of actuator powers.

Furthermore, directly implementing the contact timings optimization on the whole-body optimization framework takes greatly considerable time to solve due to the highly complexity of the problem. In our implementation, for many cases, it does not even produce a feasible solution. Therefore, these issues motivates us to take advantage of the SRB to optimize for contact timings. Section III-A will present our contact-timing optimization framework to obtain the optimal contact timings and reference trajectory, which then be used to formulate the whole-body trajectory optimization in Section III-B. The overview of our approach and control diagram is illustrated in Fig. 3.

### A. Contact timings and trajectory optimization using rigid body dynamics

To achieve a wide range of 3D jumping motions, we use rotation matrix to present the body orientation, which helps prevent singularity and unwinding issues when planning with the single rigid body dynamics [15],[18],[19]. However, using rotation matrix in the TO set up introduces more optimization variables and constraints, which causes significantly solving time. In many cases, it cannot provide a feasible solution. Thus, it is challenging and hinders the use of rotation matrix in the TO set up so far. To tackle this challenge, we propose a Taylor series approximation at a high degree to approximate the rotation matrix in  $SO(3)$  and consider an error term of rotation matrix.

Given the sequence of contacts, we will optimize their duration (i.e. contact timings). Here we choose Cartesian space to derive the SRB's equation of motion as follows:

$$\ddot{\mathbf{p}} = \sum_{s=1}^{n_s} \mathbf{f}^s/m - \mathbf{g}, \quad (1a)$$

$$\mathbf{I}_b \dot{\boldsymbol{\Omega}} + \boldsymbol{\Omega} \times \mathbf{I}_b \boldsymbol{\Omega} = \mathbf{R}^{-1} \sum_{s=1}^{n_s} \mathbf{f}^s \times (\mathbf{p} - \mathbf{p}_f^s), \quad (1b)$$

$$\dot{\mathbf{R}} = \mathbf{R} \times \boldsymbol{\Omega}, \quad (1c)$$

where  $n_s$  is number of feet,  $m$  is the robot's mass,  $\boldsymbol{\Omega} \in \mathbb{R}^3$  is angular velocity expressed in the body frame,  $\mathbf{R}$  is rotation matrix of the body frame,  $\mathbf{g}$  is the gravity acceleration;  $\mathbf{p}, \dot{\mathbf{p}}, \ddot{\mathbf{p}} \in \mathbb{R}^3$  is the COM position, velocity, acceleration of the robot's body in the world frame;  $\mathbf{f}^s \in \mathbb{R}^3$  is GRF on foot  $s^{th}$ ;  $\mathbf{p}_f^s \in \mathbb{R}^3$  is  $s^{th}$  foot position in the world frame. For the sake of notation, we define the robot's state as  $\mathbf{x} := [\mathbf{p}; \dot{\mathbf{p}}; \boldsymbol{\Omega}; \dot{\boldsymbol{\Omega}}; \mathbf{R}]$ . The contact timings and trajectory

optimization are then formulated as follows:

$$\text{minimize } \sum_{k=1}^{N^c} \epsilon_{\Omega} \boldsymbol{\Omega}_k^T \boldsymbol{\Omega}_k + \epsilon_f \mathbf{f}_k^T \mathbf{f}_k + \epsilon_R \mathbf{e}_{R_k}^T \mathbf{e}_{R_k}$$

$$\text{s.t. } \alpha(\mathbf{x}_k, \mathbf{f}_k) = 0, \quad \beta(\mathbf{x}_k, \mathbf{f}_k) \leq 0, \quad (2a)$$

$$\gamma(\mathbf{x}_k, \mathbf{x}_{k+1}, \mathbf{f}(k), \mathbf{p}_f^s(k)) = 0, \quad (2b)$$

$$\mathbf{R}_{k+1} = \mathbf{R}_k \exp(\widehat{\boldsymbol{\Omega}_k T_i / N_i}), \quad (2c)$$

$$\sum_{i=1}^n T_i \in [T_{min}, T_{max}], \quad N^c = \sum_{i=1}^n N_i \quad (2d)$$

for  $k = 1, 2, \dots, N^c$

where  $\boldsymbol{\Omega}_k \in \mathbb{R}^3$ ,  $\mathbf{f}_k \in \mathbb{R}^{12}$  is angular velocity of SRB w.r.t the body frame, and GRF on four legs at the iteration  $k^{th}$ ;  $\epsilon_{\Omega}, \epsilon_f, \epsilon_R$  are cost function weights of corresponding elements, and  $\epsilon_R, \epsilon_{\Omega} \gg \epsilon_f$ . We use error term of rotation matrix as  $\mathbf{e}_{R_k} = \log(\mathbf{R}_{ref,k}^T \mathbf{R}_k)^{\vee}$ , where  $\log(\cdot) : SO(3) \rightarrow so(3)$  is the logarithm map, and the vee map  $(\cdot)^{\vee} : so(3) \rightarrow \mathbb{R}^3$  is the inverse of hat map [17],[20]. With given final and initial rotation matrix, we utilize a linear interpolation to obtain  $\mathbf{R}_{ref,k}$  at  $k^{th}$  step. The function  $\alpha(\cdot)$  captures various constraints on initial and final body configurations. The function  $\beta(\cdot)$  captures various constraints on CoM postion, friction cone limits, GRF, and geometric constraints related to the ground and obstacle clearance. The function  $\gamma(\cdot)$  captures the dynamic constraints discretized from (1a)-(1b).

In (2d),  $n$  is a number of contact phases. For example, if the pre-selected contact schedule is four-leg contact, rear-leg contact, and flight phase, then  $n = 3$ .  $N_i$  is the predefined number of time steps for the  $i^{th}$  contact phase,  $i \in \{1, 2, \dots, n\}$ . Note that we optimize the timing  $T_i$  for each period and the total time  $T_{opt} = \sum_{i=1}^n T_i$  given predefined interval  $[T_{min}, T_{max}]$ . The equation (2c) is derived from (1c) to ensure  $\mathbf{R}_k$  evolves in the  $SO(3)$  manifold. Here,  $\exp(\cdot) : so(3) \rightarrow SO(3)$  is the matrix exponential map. It is noted that we will check a  $k^{th}$  iteration belongs to which  $i^{th}$  predefined contact phase to choose  $T_i/N_i$  accordingly.

*Remark 1:* To address the challenge that associated with the significantly solving time when utilizing rotation matrix in the TO framework, we propose the utilization of the Taylor series approximation for (2c) as follows:

$$\exp(\mathbf{A}) = \mathbf{I} + \mathbf{A} + \frac{1}{2} \mathbf{A}^2 + \frac{1}{6} \mathbf{A}^3 + \frac{1}{24} \mathbf{A}^4, \quad (3)$$

and use  $\mathbf{e}_{R_k}^T \mathbf{e}_{R_k}$  in the cost function. This approach guarantees that the rotation matrix evolves in  $SO(3)$  manifold at a reasonably accuracy and guide the TO toward a feasible solution in a fast manner.

### B. Whole-body trajectory optimization for 3D jumping

When performing highly dynamic jumping, it is important to consider the full nonlinear dynamics of the robot in the optimization framework. This will guarantee the accuracy of the jumping trajectory while transferring to the hardware.

1) *Whole-body dynamics model*: Based on the 2D non-linear dynamic model in our previous work [13], we extend it to 3D dynamics. The robot is modeled as a rigid-body system consisting of  $n$  bodies, and spatial vector algebra [21] is used to construct the robot’s equations of motion:

$$\begin{aligned} & \mathbf{H}(\mathbf{q})\ddot{\mathbf{q}} + \mathbf{C}(\mathbf{q}, \dot{\mathbf{q}})\dot{\mathbf{q}} + \mathbf{g}(\mathbf{q}) \\ & = \mathbf{B}\boldsymbol{\tau} + \mathbf{B}_{fric}\boldsymbol{\tau}_{fric}(\dot{\mathbf{q}}) + \sum_s \mathbf{J}_s^T(\mathbf{q})\mathbf{F}_s, \end{aligned} \quad (4)$$

where  $\mathbf{q} := [x; y; z; q_{roll}; q_{pitch}; q_{yaw}; \mathbf{q}_j]$  is a vector of generalized coordinates, in which  $x, y, z, q_{roll}, q_{pitch}, q_{yaw}$  are the COM position and body’s rotational angles respectively, and  $\mathbf{q}_j \in \mathbb{R}^{12}$  is a vector of joint angles. The mass matrix is denoted by  $\mathbf{H}$ ; the matrix  $\mathbf{C}$  is represented for Coriolis and centrifugal terms;  $\mathbf{g}$  is the gravity vector;  $\mathbf{J}_s$  is the spatial Jacobian of the body containing the  $s^{th}$  foot, expressed at the foot and in the world coordinate system;  $\mathbf{B}$  and  $\mathbf{B}_{fric}$  are distribution matrices of actuator torques  $\boldsymbol{\tau}$  and the joint friction torques  $\boldsymbol{\tau}_{fric}$ ;  $\mathbf{F}_s$  is the spatial force at the  $s^{th}$  foot. Moreover, for each stance foot  $s$  that is on the ground and actively supporting the robot, the following constraints are enforced :

$$\mathbf{J}_{s,stance}(\mathbf{q})\ddot{\mathbf{q}} + \dot{\mathbf{J}}_{s,stance}(\mathbf{q})\dot{\mathbf{q}} = 0. \quad (5)$$

2) *Cost function and constraints*: The goal of our framework is to find a feasible jumping motion for each 3D jumping task with the whole body dynamics. Due to the high complexity of this problem, the feasibility domain is limited. Therefore, the purpose of this cost function is to guide the optimization to converge to a feasible solution where the robot’s coordinates stays close to the reference configuration  $\mathbf{q}_{ref}$  if possible. The CoM position and body orientation obtained from Section III-A are linearly interpolated to get their profiles sampling at  $dt = 10 \text{ ms}$ , which is then used as reference for the whole-body TO here. The cost function of the trajectory optimization is defined as follows:

$$\begin{aligned} J = & \sum_{k=1}^{N-1} \epsilon_q (\mathbf{q}_k - \mathbf{q}_{ref,k})^T (\mathbf{q}_k - \mathbf{q}_{ref,k}) + \epsilon_\tau \boldsymbol{\tau}_k^T \boldsymbol{\tau}_k \\ & + \epsilon_N (\mathbf{q}_N - \mathbf{q}_N^d)^T (\mathbf{q}_N - \mathbf{q}_N^d), \end{aligned} \quad (6)$$

where  $N$  denotes the total of the time steps (i.e.  $N = T_{opt}/dt$  with  $T_{opt}$  is optimal total time obtained from Section III-A;  $\mathbf{q}_k, \boldsymbol{\tau}_k$  are the generalized coordinates and joint torque at the iteration  $k^{th}$ ;  $\mathbf{q}_N$  is the the generalized coordinates at the end of the trajectory; the first six elements of  $\mathbf{q}_{ref,k}$  is the reference COM position and body orientation obtained from the TO of SRB in Section III-A. The last 12 elements of  $\mathbf{q}_{ref,k}$  is set to be the final joint configuration. We also use  $\mathbf{q}_{ref,k}$  as initial guess for the TO to reduce the solving time.  $\epsilon_q, \epsilon_\tau, \epsilon_N$  are cost function weights of corresponding elements. Similarly to [13], we set up constraints regarding to initial and final body and joint configuration; pre-landing configuration; joint angular position and velocity limits; torque limits; friction cones; geometric constraints to ensure the body, hips, knees and swing feet have a good

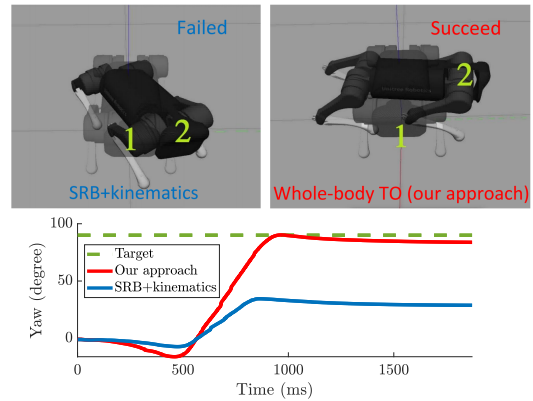


Fig. 4: Comparison between and TO of SRB+ kinematics approach and whole-body TO (our approach) for  $90^\circ$  spinning jump target.

TABLE II: Optimal contact timings, solving time via *IPOPT* for the contact timings and TO of SRB in Section III-A and whole-body TO in Section III-B

| Jumping tasks            | Optimal contact timings | Solving time timings and TO of SRB | Solving time whole-body TO |
|--------------------------|-------------------------|------------------------------------|----------------------------|
| lateral jump 30cm        | 50, 28                  | 4.14 [s]                           | 31 [s]                     |
| lateral jump down        | 52, 35                  | 5.02 [s]                           | 32 [s]                     |
| $90^\circ$ spinning jump | 56, 31                  | 5.7 [s]                            | 39 [s]                     |
| diagonal jump            | 54, 30, 33              | 5.98 [s]                           | 226 [s]                    |
| barrel roll              | 51, 32, 35              | 6.61 [s]                           | 35 [s]                     |
| double barrel roll       | 52, 34, 45              | 11.7 [s]                           | 46 [s]                     |
| double backflip          | 50, 33, 69              | 7.23 [s]                           | 89 [s]                     |

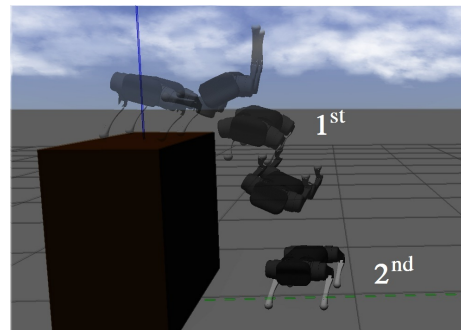


Fig. 5: A **double barrel roll** from a box of height  $0.8\text{m}$  with our proposed framework.

clearance with other robot’s parts, with the ground, and with obstacle clearance. These constraints are enforced based on the optimal contact timings obtained from Section III-A.

#### IV. JUMPING AND LANDING CONTROLLER

Having introduced the whole-body TO approach, in this section we present a jumping and landing controller to help robot tracking the reference trajectory and handle the high impact with the ground (see Fig.3). The desired joint angle  $\mathbf{q}_d$ , joint velocity  $\dot{\mathbf{q}}_d$ , foot position  $\mathbf{p}_{f,d}$  and foot velocity  $\mathbf{v}_{f,d}$  w.r.t their hips, and feed-forward joint torque  $\boldsymbol{\tau}_d$  are obtained from the whole-body TO. They are then linearly interpolated to get new reference profiles at  $1 \text{ kHz}$ . To track the reference trajectories, we use the feedback Cartesian PD

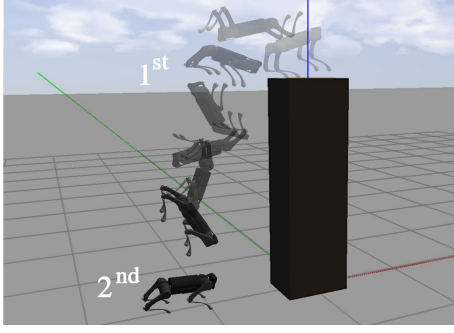


Fig. 6: A double backflip from a box of height 2m with our proposed framework

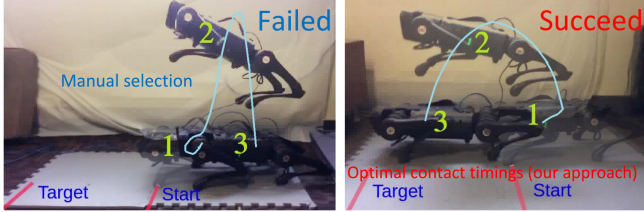


Fig. 7: Motion snapshots from jumping forward with manual selection of contact timings in the left figure and optimal contact timings (our approach) in the right figure.

controller that executes at 1 kHz:

$$\tau_{ff} = \mathbf{J}(\mathbf{q}_j)^\top [\mathbf{K}_p(\mathbf{p}_{f,d} - \mathbf{p}_d) + \mathbf{K}_d(\mathbf{v}_{f,d} - \mathbf{v}_f)] + \tau_d$$

where  $\mathbf{J}(\mathbf{q}_j)$  is the foot Jacobian at the configuration  $\mathbf{q}_j$ ;  $\mathbf{K}_p$  and  $\mathbf{K}_d$  are diagonal matrices of proportional and derivative gains. The joint PD controller running at 10 kHz in the low-level motor control is integrated to improve the tracking performance. The full controller for tracking desired trajectories is:

$$\tau = \tau_{ff} + \mathbf{K}_{p,joint}(\mathbf{q}_{j,d} - \mathbf{q}) + \mathbf{K}_{d,joint}(\dot{\mathbf{q}}_{j,d} - \dot{\mathbf{q}}). \quad (7)$$

Since there always exists a model mismatch between the optimization and hardware, it normally has orientation angle errors upon landing. Therefore, we utilize a real-time landing controller to handle impact, control GRF, balance the whole body motion during the landing phase, and recover the robot from unexpected landing configurations. For that controller, we extend the proposed QP controller presented in [13] for the 3D jumping motions.

**if** (any  $c_s \geq \delta$ ) & ( $t \geq T_{posing}$ )  
**then** switch to landing controller,

where  $c_s$  is the value obtained from the contact sensor of the foot  $s^{th}$ , and  $\delta$  is the force threshold to determine if the ground impact happened.  $T_{posing}$  is the instant at the beginning of the pre-landing configuration (after that instant the desired joint velocity  $\dot{\mathbf{q}}_j^d = 0$ ). When the impact is detected in any foot, we switch from jumping controller to landing controller, then based on which feet are in contact, different robot models are used for the landing controller. Our experimental results validate that it is effective to use

the QP landing controller for SRB to handle impact with the ground and balance the robot when landing.

*Remark 2:* Normally, all legs are not in ground simultaneously due to the mismatch between the optimization model and hardware. Hence, utilizing a controller for swing legs also plays a crucial role here. Based on the contact model derived from the contact detection, the swing legs during landing phase are set at zero normal force and kept at the pre-landing configuration using PD controller until the ground contact is detected on these legs to prevent excessive impact force and unnecessarily extended movement.

## V. RESULTS

This section presents results from experimental testing and simulation with the A1 robot. A video of the results is included as supplementary material.

### A. Numerical Simulation

We use MATLAB and CasADi (see [22]) to construct and solve all presented TO approaches for all 3D jumping behaviors. It is flexible to predefine the contact sequence according to the user's preference. Here, for the lateral and spinning jumps, we use four-leg contact and flight schedule, while we utilize the four-leg contact, two-leg contact, and flight schedule for the other jumps. The contact timings and trajectory optimization of SRB model is solved in a fast manner for all 3D jumps, and the whole-body TO is solved at reasonable time given the high complexity of the WBD model as shown in Table II.

We implement the TO of SRB dynamics+kinematic constraints to make comparisons with our proposed whole-body TO for various 3D jumps. The TO of SRB dynamics+kinematics constraints is constructed based on (2), but we use joint space instead of Cartesian space to enforce related kinematic constraints. The joint torque is not an optimization variable, which finds similar to the TO approach presented in [9]. Among the comparisons, we pick a spinning jump  $90^\circ$  to discuss here. As we can see in Fig. 4, while our approach using the whole-body TO guarantees a highly accurate jump, the TO framework with SRB and kinematics constraints fails to generate any significant yaw motion.

Moreover, we have also successfully validated our approach for highly complex 3D dynamic jumps such as double backflip and double barrel jump from a high table (see Fig. 5&6). These results also prove the effectiveness of the landing controller in robustly recovering the body configuration under greatly hard impact with the ground.

### B. Experimental Validation

We have also successfully validated our approach in the robot hardware. Firstly, we make a comparison between optimal contact timings and manually selected contact timings. We pick the experiment with jumping forward 0.6 m with the contact sequence of four-leg contact, rear-leg contact and flight to discuss here. Their results are illustrated in Fig. 7 and Fig. 8. If contact timings are manually selected with unnecessary long flight time (e.g., 550 ms), this makes the

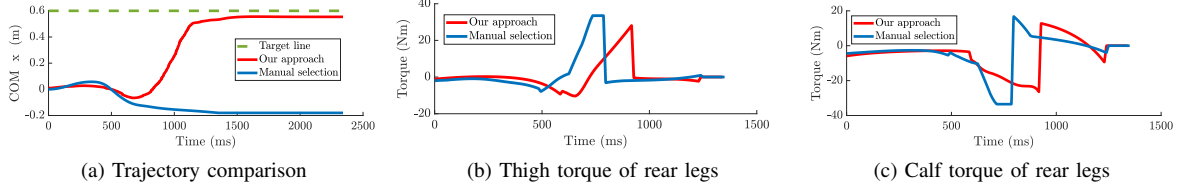


Fig. 8: **Comparison between manual selection and optimal contact timings (our approach)** The comparison is considered based on target achievement from experiments in Fig. 8a, and the feed forward torque of rear legs generated from the whole-body TO for jumping forward  $0.6\text{ m}$  under manual selection of contact timings and optimal contact timings (our approach) in Fig. 8b & 8c. The Fig. 8 is accompanied with the Fig. 7.



Fig. 9: **Experiments:** Motion snapshots from a successful 3D diagonal jump  $[x, y, yaw] = [0.4\text{ m}, -0.3\text{ m}, 45^\circ]$  from a side and a top view.

motor’s torque saturated in  $100\text{ ms}$  that is up to  $1/3$  of rear-leg contact phase. This seriously affects the motor working condition, causing failed joint tracking performance. Thus, the robot is unable to reach the target. On the other hand, selecting too small flight time makes the optimization unsolvable since the robot does not have enough power to jump to the desired configuration. By using optimal contact timings, we are able to prevent the torque saturation issue and guarantees the successful jump on the robot hardware. Secondly, we present the results of different 3D jumping experiments on the A1 robot, including a diagonal jump or a barrel roll from a high box. We pick some jumping tasks to discuss here. In a successful diagonal jump (see Fig. 9), the jumping controller guarantees the high tracking performance and the landing controller is able to handle the impact with the ground as evident in Fig. 10. Using our approach, the robot can successfully performs a barrel roll from a box of height  $0.4\text{ m}$  in experiments (see Fig. 1). This result illustrates the efficiency of our approach in optimizing contact timings for the jumping task as well as the accuracy of the optimization framework while transferring the result to the real hardware. In addition, this also validates the effectiveness of the landing controller. In this experiment, since the robot rotates with high angular acceleration from the high altitude, it has a considerably hard impact with the ground. As illustrated in Fig. 11, the landing controller computes reasonable force command to robustly recover the whole body position and orientation under hard impact and error of landing configuration. Fig. 11 shows trajectories of the body position and orientation along with force command during the landing phase.

## VI. CONCLUSIONS

This paper has introduced the framework for performing highly dynamics 3D jumps on quadruped robots that require model accuracy, perfect timings and coordination of the whole body motion. This framework combines timings

and TO of SRB dynamics, whole-body TO, the jumping controller and robust landing controller. The efficiency of the framework is validated via both A1 robot model and experiments on performing these aggressive tasks. The vision to autonomously detect obstacles will be integrated with the proposed framework in our future work.

## ACKNOWLEDGMENTS

The authors would like to thank Yiyu Chen and Hiep Hoang at Dynamic Robotics and Control lab for their assistance in simulation and hardware experimentation. Chuong also thank Dr. Roy Featherstone for the discussion about Spatial v2 for rigid body dynamics.

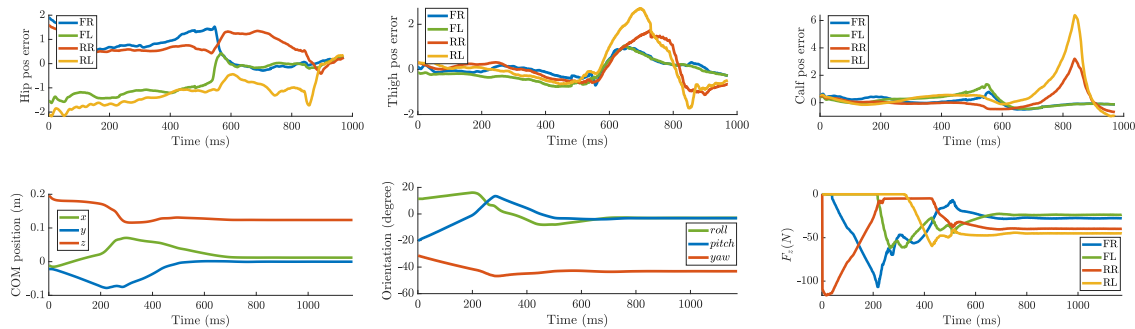


Fig. 10: **3D diagonal jump in experiments.** The upper figures are the tracking error of joint positions (degree) with jumping controller, and the lower figures are the COM position, body orientation, and force command from landing controller during the landing phase, when the robot performs a diagonal jump (see Fig. 9). FR, FL, RR and RL are used to denote front right, front left, rear right and rear left leg respectively.

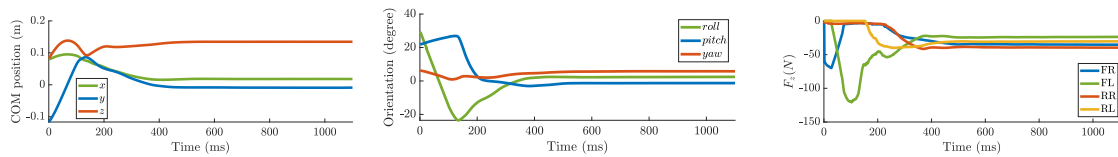


Fig. 11: **Landing controller for a barrel jump in experiments** This plots show the COM position, body orientation, and force command during the landing phase when the robot performs a barrel roll from a box with the height of 0.4 m (see Fig. 1).

## REFERENCES

- [1] Q. Nguyen, A. Hereid, J. W. Grizzle, A. D. Ames, and K. Sreenath, "3d dynamic walking on stepping stones with control barrier functions," in *IEEE 55th Conference on Decision and Control (CDC)*, pp. 827–834, 2016.
- [2] Q. Nguyen, A. Agrawal, X. Da, W. C. Martin, H. Geyer, J. W. Grizzle, and K. Sreenath, "Dynamic walking on randomly-varying discrete terrain with one-step preview," *Robotics: Science and Systems*, vol. 2, no. 3, 2017.
- [3] Q. Nguyen, X. Da, J. Grizzle, and K. Sreenath, "Dynamic walking on stepping stones with gait library and control barrier functions," *Algorithmic Foundations of Robotics XII*, pp. 384–399, 2020.
- [4] Y. Gong, R. Hartley, X. Da, A. Hereid, O. Harib, J.-K. Huang, and J. Grizzle, "Feedback control of a cassie bipedal robot: Walking, standing, and riding a segway," in *2019 American Control Conference (ACC)*, pp. 4559–4566, IEEE, July 2019.
- [5] M. Raibert, K. Blankespoor, G. Nelson, R. Playter, and the Big-Dog Team, "Bigdog, the rough-terrain quaduped robot," in *Proceedings of the 17th World Congress*, pp. 10822–10825, 2008.
- [6] Y. Ding and H.-W. Park, "Design and experimental implementation of a quasi-direct-drive leg for optimized jumping," in *Intelligent Robots and Systems (IROS), 2017 IEEE/RSJ International Conference on*, pp. 300–305, IEEE, 2017.
- [7] H.-W. Park, P. M. Wensing, and S. Kim, "Jumping over obstacles with mit cheetah 2," *Robotics and Autonomous Systems*, vol. 136, p. 103703, 2021.
- [8] D. W. Haldane, M. Plecnik, J. K. Yim, and R. S. Fearing, "Robotic vertical jumping agility via series-elastic power modulation," *Science Robotics*, vol. 1, no. 1, 2016.
- [9] M. Chignoli, "Trajectory optimization for dynamic aerial motions of legged robots," Master's thesis, MIT, 2021.
- [10] G. Bledt, M. J. Powell, B. Katz, J. Di Carlo, P. M. Wensing, and S. Kim, "Mit cheetah 3: Design and control of a robust, dynamic quadruped robot," in *2018 IEEE/RSJ International Conference on Intelligent Robots and Systems (IROS)*, pp. 2245–2252, IEEE, 2018.
- [11] M. Hutter, C. Gehring, D. Jud, A. Lauber, C. D. Bellicoso, V. Tsounis, J. Hwangbo, K. Bodie, P. Fankhauser, M. Bloesch, R. Diethelm, S. Bachmann, A. Melzer, and M. Hoepflinger, "ANYmal - a highly mobile and dynamic quadrupedal robot," in *IEEE/RSJ International Conference on Intelligent Robots and Systems*, pp. 38–44, Oct 2016.
- [12] D. Kim, J. D. Carlo, B. Katz, G. Bledt, and S. Kim, "Highly dynamic quadruped locomotion via whole-body impulse control and model predictive control," in *arXiv preprint arXiv:1909.06586*, 2019.
- [13] Q. Nguyen, M. J. Powell, B. Katz, J. D. Carlo, and S. Kim, "Optimized jumping on the mit cheetah 3 robot," in *2019 International Conference on Robotics and Automation (ICRA)*, pp. 7448–7454, IEEE, 2019.
- [14] J. Di Carlo, P. M. Wensing, B. Katz, G. Bledt, and S. Kim, "Dynamic locomotion in the mit cheetah 3 through convex model-predictive control," in *2018 IEEE/RSJ International Conference on Intelligent Robots and Systems (IROS)*, pp. 1–9, IEEE, 2018.
- [15] Y. Ding, A. Pandala, and H.-W. Park, "Real-time model predictive control for versatile dynamic motions in quadrupedal robots," in *2019 International Conference on Robotics and Automation (ICRA), Montreal, Canada*, pp. 8484–8490, IEEE, May 2019.
- [16] A. W. Winkler, C. D. Bellicoso, M. Hutter, and J. Buchli, "Gait and trajectory optimization for legged systems through phase-based end-effector parameterization," *IEEE Robotics and Automation Letters*, vol. 3, pp. 1560–1567, 2018.
- [17] T. Lee, M. Leoky, and N. H. McClamroch, "Geometric tracking control of a quadrotor uav on se(3)," in *49th IEEE Conference on Decision and Control (CDC)*, pp. 5420–5425, Dec 2010.
- [18] M. D. Shuster, "A survey of attitude representations," *Navigation*, vol. 8, no. 9, pp. 439–517, 1993.
- [19] S. P. Bhat and D. S. Bernstein, "A topological obstruction to continuous global stabilization of rotational motion and the unwinding phenomenon," *Systems & Control Letters*, vol. 39, no. 1, 2000.
- [20] F. Bullo and A. D. Lewis, "Geometric control of mechanical systems: modeling, analysis, and design for simple mechanical control systems," *Springer Science & Business Media*, vol. 49, 2004.
- [21] R. Featherstone, *Rigid body dynamics algorithms*. Springer, 2014.
- [22] J. A. E. Andersson, J. Gillis, G. Horn, J. B. Rawlings, and M. Diehl, "CasADi – A software framework for nonlinear optimization and optimal control," *Mathematical Programming Computation*, In Press, 2018.